Characteristic Impedance Extraction Using Calibration Comparison

S. Vandenberghe, D. Schreurs, G. Carchon*,
B. Nauwelaers, W. De Raedt*

Personal use of this material is permitted. However, permission to reprint/replublish this material for advertising or promotional purposes or for creating new collective works for resale or redistribution to servers or lists or to reuse any copyrighted component of this work in other works must be obtained from the IEEE.

The following preprint differs from the final publication:

S. Vandenberghe, D. Schreurs, G. Carchon, B. Nauwelaers, W. De Raedt, "Characteristic Impedance Extraction Using Calibration Comparison," *IEEE Transactions on Microwave Theory and Techniques,* vol. 49, no. 12, December 2001, pp. 2573–2579.

Characteristic Impedance Extraction Using Calibration Comparison

S. Vandenberghe, D. Schreurs, G. Carchon*,
B. Nauwelaers, W. De Raedt*

Index Terms – Impedance measurement, coplanar waveguides.

Abstract – A robust line impedance identification method is presented. It determines the characteristic impedance of on-wafer TLR standards measured after an initial off-wafer LRM or TLR calibration. The only assumption made is that the obtained trans-wafer error boxes are a cascade of a symmetric probe related disturbance and a change in reference impedance. The proposed method yields an unbiased estimate of the complex characteristic impedance. Results from coplanar lines on a medium resistivity silicon substrate support the made assumption.

1 Introduction

The TLR method is often the most feasible on-wafer calibration technique since it only requires two lines of a different length[1]. A drawback is that the recovered reflection parameters are at an unknown reference impedance, set by the characteristic line impedance. An indirect determination using the propagation constant is only possible for low loss substrates[2].

Calibration comparison methods measure on-wafer TLR standards after an initial off-wafer calibration at a known reference impedance. The obtained trans-wafer error boxes are then identified with an equivalent circuit, modelling the contact geometry and substrate change, and a transformer [3][4]. This transformer accounts for the change in voltage over the virtual two port junction if the reference impedance at both ports is chosen equal. An example is the waveguide TE_{10} E-plane step junction[5, p. 162] where the port impedance is chosen and the modal voltage is determined from power consistency. For ideal transmission line discontinuities it is, however, more physically consistent to assume a constant voltage over the junction. This condition determines the port 2 modal voltage, reference impedance, and removes the transformer.

Both interpretations result in the same voltage normalized S-parameter values if the transformer ratio $n = \sqrt{Z_s/Z_l}$. The normalization follows implicitely from the reciprocity condition $S_{n21} = S_{n12}$ as

$$\frac{Y_{21}}{Y_{12}} = 1 \quad \Rightarrow \quad \frac{S_{n21}}{S_{n12}} = \frac{S_{21}\sqrt{\frac{Z_{c1}}{Z_{c2}}}}{S_{12}\sqrt{\frac{Z_{c2}}{Z_{c1}}}} = 1 \tag{1}$$

The authors are with the K.U.Leuven ESAT TELEMIC, Kasteelpark Arenberg 10, B–3001 Leuven, Belgium, and with *IMEC MCP, Kapeldreef 75, B–3001 Leuven, Belgium.

shows.

2 Reciprocity

Reciprocity of a two-port junction is a necessary condition for the determination of the forward and reverse transmission if only their product is known, as obtained from e.g. SOL or TLR calibration techniques. Equating both quantities[5, p. 159] is not always valid[6].

The voltage S-parameter circuit representation is a compact way of describing an underlying field problem. A normalization relates the field with a macroscopic incident and reflected voltage or current. For TE or TM modes in a reciprocal uniform medium, the fields at port i satisfy[5, p. 72]

$$\begin{aligned}[\vec{E}_i, \vec{H}_i] &= [\vec{e}_{ti} + \vec{e}_{zi}, \vec{h}_{ti} + \vec{h}_{zi}]C_{0i}^{+}e^{-\gamma z} \\ &\quad + [\vec{e}_{ti} - \vec{e}_{zi}, -\vec{h}_{ti} + \vec{h}_{zi}]C_{0i}^{-}e^{\gamma z}\end{aligned} \tag{2}$$

with $\vec{e}, \vec{h}$ the z-independent modal fields and C_0^+, C_0^- the two wave amplitude constants. An arbitrary transversal field follows from

$$\vec{E}_{ti} = \left(\frac{V_{0i}^{+}}{V_{ci}}e^{-\gamma_i z} + \frac{V_{0i}^{-}}{V_{ci}}e^{\gamma_i z}\right)\vec{e}_{ti} = \frac{V_i(z)}{V_{ci}}\vec{e}_{ti} \tag{3}$$

$$\vec{H}_{ti} = \left(\frac{I_{0i}^{+}}{I_{ci}}e^{-\gamma_i z} - \frac{I_{0i}^{-}}{I_{ci}}e^{\gamma_i z}\right)\vec{h}_{ti} = \frac{I_i(z)}{I_{ci}}\vec{h}_{ti} \tag{4}$$

with V_c and I_c the modal voltage and current. The wave voltages at port i, V_0^+ and V_0^-, determine the field since

$$Z_{ci} = \frac{V_{ci}}{I_{ci}} = \frac{V_{0i}^{+}}{I_{0i}^{+}} = \frac{V_{0i}^{-}}{I_{0i}^{-}} \tag{5}$$

holds from (2).

The Lorentz reciprocity theorem[5, pp. 57–59, 159] applied on a two-port source free junction, e.g. fig. 1, imposes a condition on the incident and reflected fields. The Lorentz integral

$$\oint_A (\vec{E}^I \times \vec{H}^{II} - \vec{E}^{II} \times \vec{H}^I)\mathrm{d}\vec{A} = 0 \tag{6}$$

reduces to the two terminal planes if the remaining enclosing surface is characterized by a scalar surface impedance or is infinitely far away. Choosing current sources outside of the junction such that $\vec{E}_{t2}^{I} = 0$, experiment I, and such that $\vec{E}_{t1}^{II} = 0$, experiment II, and substituting with (3–4) yields a reciprocity factor

$$K_i = \frac{1}{V_{ci}I_{ci}}\int_{A_i} \vec{e}_{ti} \times \vec{h}_{ti} \cdot \vec{u}_z \mathrm{d}A \tag{7}$$

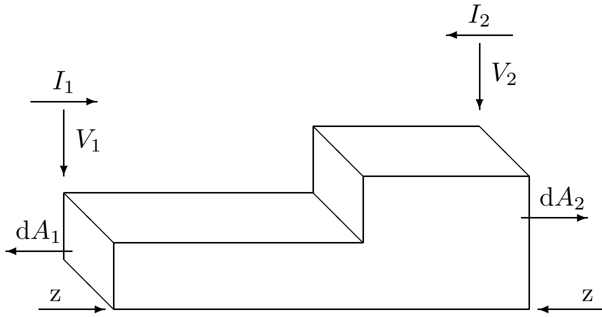

Figure 1: A TE_{10} E-plane step waveguide junction as an example of a reciprocal microwave circuit.

and with (5) results in

$$\frac{Y_{21}}{Y_{12}} = \frac{K_1}{K_2} \quad \Leftrightarrow \quad D = \frac{S_{21}}{S_{12}} = \frac{Z_{c2}K_1}{Z_{c1}K_2} \tag{8}$$

which agrees with [6, eq. 22]. The Z_c dependence of the reciprocity ratio D is removed using the normalized quantities $V_n^{\pm} = V^{\pm}/\sqrt{Z_c}$ which yields

$$D_n = \frac{S_{n21}}{S_{n12}} = \frac{S_{21}\sqrt{\frac{Z_{c1}}{Z_{c2}}}}{S_{12}\sqrt{\frac{Z_{c2}}{Z_{c1}}}} = \frac{K_1}{K_2} \tag{9}$$

with S_n the "voltage" normalized S-parameters. Note that calculating $S_{n21} = S_{n12} = \sqrt{S_{21}S_{12}}$ implicitely chooses $V_n^{\pm} = V^{\pm}/\sqrt{Z_c/K}$.

The power carried by the forward modal field agrees with the macroscopic voltage current power if

$$S_{ci} = \frac{1}{2}\int_{A_i} \vec{e}_{ti} \times \vec{h}_{ti}^{*} \cdot \vec{u}_z \mathrm{d}A = \frac{1}{2}V_{ci}I_{ci}^{*} \tag{10}$$

holds. This power consistency determines the phase of Z_c[7] and sets K_i to unity for TE or TM modes, if $[V_c, I_c]$ are in phase with $[\vec{e}_t, \vec{h}_t]$. A line integral defining V_c or a contour integral defining I_c, for TM or TE modes, in the z-plane satisfies this condition.

3 Error box normalization

A trans-wafer error box relates an off- to on-wafer calibration. The reciprocity ratio is calculated assuming an initial coaxial calibration. Performing an off- and on-wafer calibration determines two sets error boxes, S_x^I and S_x^{II} with $x = [a, b]$, and two sets deembedded S-parameters, S_D^I and S_D^{II}. The data satisfies

$$S_D^{coax} = S_a^I \| S_D^I \| \overline{S_b^I} = S_a^{II} \| S_D^{II} \| \overline{S_b^{II}} \tag{11}$$

with $\|$ the cascade operator, the reversing overbar as

$$\overline{S} = \begin{bmatrix} 0 & 1 \\ 1 & 0 \end{bmatrix} S \begin{bmatrix} 0 & 1 \\ 1 & 0 \end{bmatrix}, \tag{12}$$

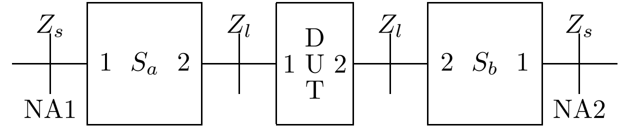

Figure 2: The TLR error box port numbering. The port 2 reference impedance is set by the line impedance.

and the port numbering from fig. 2. Rewriting (11) gives

$$S_D^I = 1/S_a^I \| S_a^{II} \| S_D^{II} \| \overline{S_b^{II}} \| 1/\overline{S_b^I} \tag{13}$$

with $1/S$ the S-parameter deembedding matrix. The matrices

$$S_a = 1/S_a^I \| S_a^{II} \qquad S_b = 1/S_b^I \| S_b^{II} \tag{14}$$

describe the on- to off-wafer S-parameter transformation. The reciprocity ratio of these trans-wafer error boxes is

$$D_x = \frac{S_{x21}}{S_{x12}} = \frac{D_x^{II}}{D_x^I} = \frac{K_{x2}^I}{K_{x2}^{II}} \tag{15}$$

using the port numbering in fig. 2 and the normalization from (9). The ratio D_x is unity if the off- and on-wafer factors K are equal, and is independent of the coax calibration.

Linear calibration algorithms, e.g. TLR and LRM, recover the reflection coefficients and an estimate of

$$S_{a21}S_{a12} \approx k_1 \qquad S_{b21}S_{b12} \approx k_2 \tag{16}$$
$$S_{a21}S_{b12} \approx k_3 \qquad S_{b21}S_{a12} \approx k_4 \tag{17}$$

for the transmission coefficients[8]. The ratio

$$\frac{D_b}{D_a} \approx \frac{k_4}{k_3} \tag{18}$$

is also determined. This 7-term linear calibration is converted into an 8-term absolute calibration through the estimation of one factor. A solution, for reciprocal error boxes with a reciprocity ratio of unity, is to determine S_{a21} such that $D_a \approx 1 \approx D_b$, thus choosing voltage normalized S-parameters. An exact solution requires that (18) equals unity. A practical approach is to distribute the error over D_a and D_b using

$$D_a D_b = 1 \quad \Rightarrow \quad D_a = s_1\sqrt{k_3/k_4} \tag{19}$$
$$\Rightarrow \quad S_{a21} = s_2\sqrt{k_1 D_a}\,. \tag{20}$$

The sign $s_i = \pm 1$ is chosen such that the obtained value approximates $e^{-j\omega\tau_i}$, where τ_i is an adaptive estimation from previous frequency points with an initial value zero. The reciprocity error $|D_x - 1|$ is typically lower than 10^{-3} for good measurements.

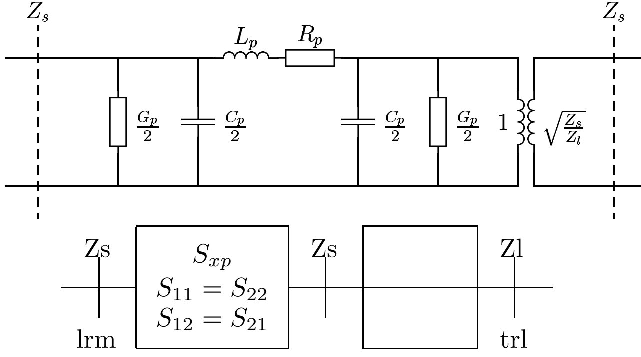

Figure 3: The error box model used for the characteristic impedance identification. Top: the equivalent circuit. Bottom: the reflection parameter based model. The S-parameter response follows from the cascade of a symmetric probe related disturbance S_{xp} and an impedance change from Z_s to Z_l.

$\vec{x} =$	$\vec{v}_1$	$\vec{v}_2$	$\vec{v}_3$	$\vec{v}_4$	$\vec{v}_5$	$\vec{v}_6$
$\Re(Z_l)$					-1.0	
$\Im(Z_l)$						-1.0
$\Re(S_{ap11})$	.17	.65	$-.72$	.20		
$\Im(S_{ap11})$	$-.65$	.17	.20	.72		
$\Re(S_{ap12})$	.20	.72	.65	$-.17$		
$\Im(S_{ap12})$	$-.72$	.20	$-.17$	$-.65$		
s_{ii}	1.5	1.5	1.4	1.4	0.01	0.01

Table 1: The vectors $\vec{v}_i$ and their associated singular value for the linearized one error box identification problem. Measured S-parameters at 10 GHz from the structures in fig. 10 were used. The identified exact solution is $Z_l = 51.7 + j7.6$ Ohm, $S_{ap11} = -0.01 - j0.01$ and $S_{ap12} = 0.98 - j0.02$, if $Z_s = 50$ Ohm.

4 Error box identification

The trans-wafer error box $x = \{a, b\}$ is modelled by a symmetric probe related disturbance S_{xp} cascaded by a change in reference impedance from Z_s to Z_l, see fig. 3. The S-parameters follow from

$$S_x^{cir} = \begin{bmatrix} S_{xp11} & S_{xp12} \\ S_{xp12} & S_{xp11} \end{bmatrix} \| S_z(Z_s, Z_l) \quad (21)$$

$$S_z = \frac{1}{Z_{02} + Z_{01}} \cdot \begin{bmatrix} Z_{02} - Z_{01} & 2\sqrt{Z_{01}Z_{02}} \\ 2\sqrt{Z_{01}Z_{02}} & -Z_{02} + Z_{01} \end{bmatrix} \quad (22)$$

with $S_z(Z_{01}, Z_{02})$ the response of a thru in a Z_{01}/Z_{02} environment. Equating simulated and measured S-parameters for M error boxes yields $8M$ real equations,

$$\vec{f}(\vec{x}) = \begin{bmatrix} \vdots \\ \Re(S_{xij}^{cal} - S_{xij}^{cir}) \\ \Im(S_{xij}^{cal} - S_{xij}^{cir}) \\ \vdots \end{bmatrix} = \vec{0}\,, \quad (23)$$

of which $6M$ are independent due to reciprocity. There are $4M + 2$ real unknowns since Z_s is known and Z_l is equal for all error boxes.

The linearization of $\vec{f}(\vec{x})$ in the solution reveals the sensitivity information. The jacobian is rewritten as $J = USV^T$ by the singular value decomposition, with $U = [\ldots \vec{u}_i \ldots]$ and $V = [\ldots \vec{v}_i \ldots]$ orthonormal and S a diagonal matrix of singular values s_i. From

$$\Delta\vec{f} \approx J\Delta\vec{x} = USV^T\Delta\vec{x} \quad (24)$$

follows that the penalty $\|\Delta\vec{f}\|$ for adding $\vec{v}_i$ to the solution is given by $\|J\vec{v}_i\| = s_i$. Table 1 summarizes the results for one trans-wafer error box modelling a cpw discontinuity at 10 GHz. The estimation of Z_l is decoupled from the probe parasitics S_{xp}, which is true as long as the probe disturbance is small. The singular values indicate that $\vec{f}$ is more sensitive for the probe related unknowns. A noticeable faster convergence of the Newton-Rhapson zero solving algorithm for S_{xp}, compared to Z_l, may thus be explained.

5 A bidirectional search

The iterative solution of $\vec{f}(\vec{x}) = \vec{0}$ searches for all unknowns simultaniously and is a forward search method. Direct extraction, backward search, methods calculate unknown per unknown from selected measurements. A bidirectional search approach[9] was implemented to exploit the sensitivity difference and to reduce the number of unknowns from $4M + 2$ to 2. The line impedance Z_l is the ordinary optimization unknown, and the probe disturbance is extracted as follows: for every port x

1. calculate S_z and $S_{z,inv} = S_z(Z_l, Z_s)$ from Z_l, with $\vec{x} = [\Re(Z_l); \Im(Z_l)]$,
2. recover the probe response from the measurements S_x^{cal} using $S_{xp}^{rec} = S_x^{cal} \| S_{z,inv}$,
3. extract a better estimate with

$$S_{xp11}^{est} = (S_{xp11}^{rec} + S_{xp22}^{rec})/2 \quad (25)$$

$$S_{xp12}^{est} = (S_{xp12}^{rec} + S_{xp21}^{rec})/2\,, \quad (26)$$

4. calculate $S_x^{cir} = S_{xp}^{est} \| S_z$,
5. evaluate (23) and add the 8 results to $\vec{f}$.

Repeating this procedure M times yields $8M$ equations. The condition of the linearized problem reduces to unity, indicating equal sensitivity for the real and imaginary part of Z_l. The internal condition is, however, unchanged and the probe related unknowns are still extracted with higher accuracy. The cost function for two trans-wafer error

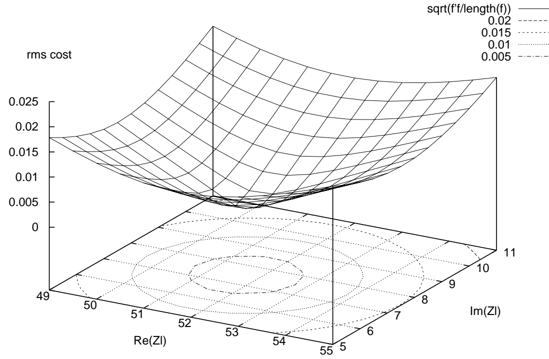

Figure 4: The rms cost of the bidirectional search method. A clear distinct minimum with equal sensitivity for the real and imaginary part is centered around the least squares solution $Z_l = 51.7 + j7.6$. The two error box experimental data is from the structures in fig. 10, at 10 GHz.

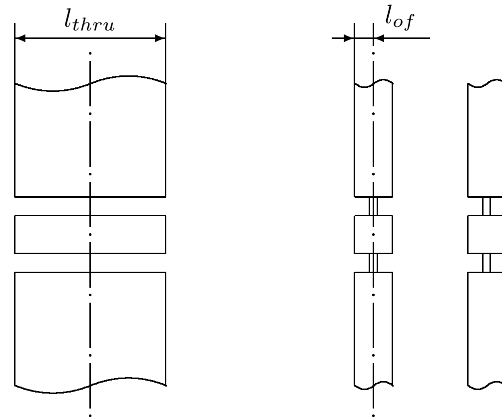

Figure 5: Typical probe standards present on a coplanar LRM calibration substrate. The recovered S-parameters are at a reference plane in the center of the thru (left). The reference impedance is set by the probe tip load response (right), calculated at the reference plane.

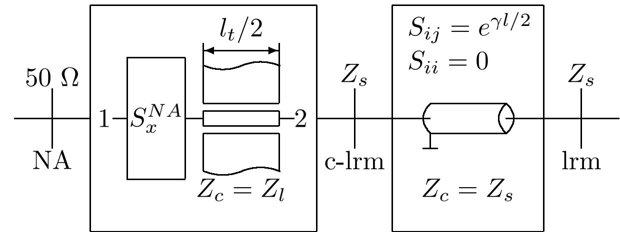

Figure 6: A probe tip LRM calibration corrects for a non zero length thru by shifting the reference plane from the center of the thru to the probe tip. Numerically, the zero length thru error box (left) is cascaded by a negative delay transmission line (right). This correction is approximative if $Z_s \neq Z_l$ but does not change the reference impedance Z_s.

boxes, fig. 4, shows a well defined minimum. Robustness and convergence speed improve due to the efficient estimation (25) of the usually low probe reflections.

6 LRM offset compensation

Calibration comparison methods rely on the accurate knowledge of the off-wafer reference impedance Z_s since only the ratio Z_l/Z_s is independently estimated, as follows from e.g. (22). Off-wafer LRM is broadband but high frequency accuracy is limited by the imperfect match standard. Moreover, most coplanar calibration substrates use a non zero length thru combined with probe tip loads, as in fig. 5. This offset change introduces an error if the thru line and load impedance differ.

The LRM algorithm employs a match standard to determine the error box port 1 reflection S_{x11}, see fig. 2. Further completion establishes a port 2 reference plane in the center of the thru if its delay is assumed zero. By definition, the calibration reference impedance Z_s is the load by which port 2 is terminated such that the input reflection equals S_{x11}. Thus, Z_s is the match impedance Z_m recalculated at the reference plane.

A probe tip LRM calibration uses a specified delay and loss to shift the reference plane from the center of the thru to the probe tip. The thru is assumed reflection free and fully characterized by its total propagation constant γl. Actually, the algorithm cascades the zero length thru error box, see fig. 6, by a negative delay transmission line at port 2. The zero reflection assumption sets the characteristic impedance of this line equal to Z_s. This correction is approximative if the thru line impedance Z_l differs from Z_s, yielding remnant probe parasitics, but the reference impedance remains unchanged.

In both cases, the LRM reference impedance Z_s equals the match impedance Z_m calculated at the reference plane in the center of the thru. For a probe tip load follows Z_s from a cascade of a negative length thru line terminated in Z_m. The match impedance $Z_m(z = 0)$ relates to $Z_s(z)$ measured at position z along the thru line using the deembedding formula

$$z_m = \frac{Z_m}{Z_l} = \frac{z_s + \mathrm{tgh}(\gamma z)}{1 + z_s \mathrm{tgh}(\gamma z)} \tag{27}$$

with

$$z_s = \frac{Z_s}{Z_l} \qquad z = -(l_{of} - l_{thru}/2)\,. \tag{28}$$

The unknowns γ and z_s are obtained from an LRM followed by a TLR calibration on the same wafer, with all lines equal in transverse geometry. Impedance identification applied on these LRM to TLR trans-calibration error boxes yields z_s, and z_m via (27). The estimation of Z_l via Z_m/z_m is independent of the offset error between the match and the thru reference plane. A virtual load response Z_s then follows from z_s.

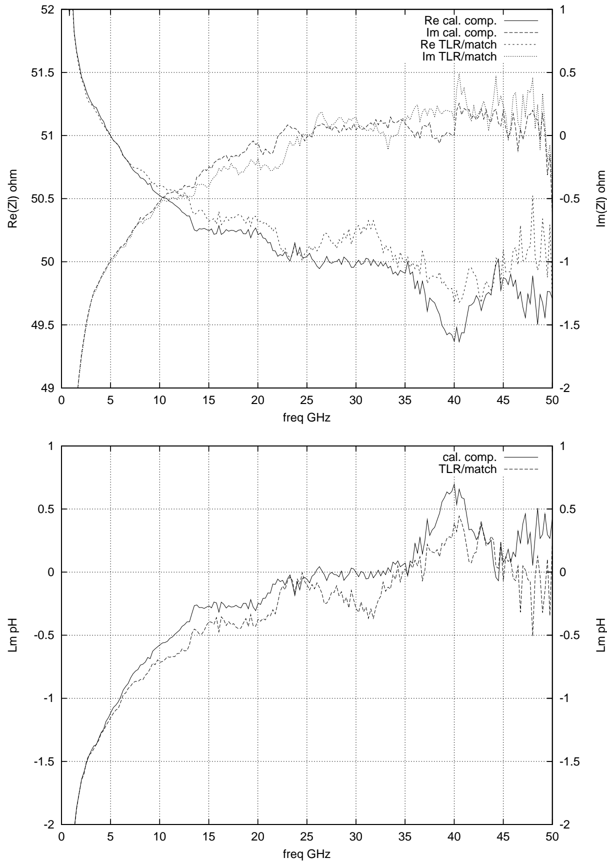

Figure 7: Top: the extracted line impedance using the new technique and the TLR/match method. Bottom: the series inductance of the virtual load at the reference plane, in the center of a 197.4 μm thru with $l_{of} = 25.4$ μm, for the two methods. This inductance models the probe tip to reference plane offset error. The load itself is assumed equal to 50 Ohm. The error boxes were calculated using an initial probe tip LRM calibration as reference, followed by multi-line TLR on the same alumina calibration substrate.

An alternative approach is to perform a TLR calibration and to contact the match standard. This TLR/match method measures the normalized impedance z_m, and z_s then follows from (27). Both methods allow for the determination of Z_l and Z_s if Z_m is known.

7 Experiment

The network analyzer was calibrated by an off-wafer probe tip LRM calibration on a Cascade 101-190 coplanar alumina substrate. The thru loss and delay, 32 GΩ/s and 1.13 ps, were estimated from the available lines. Multi-line TLR was used to calculate the LRM to TLR error boxes. The effect of the match offset error was estimated by setting the probe tip load to 50 Ohm, see fig. 7. The resulting error, a load inductance of about -0.5 pH around 14 GHz, is limited to $j0.04$ Ohm below 35 GHz. Agreement of the

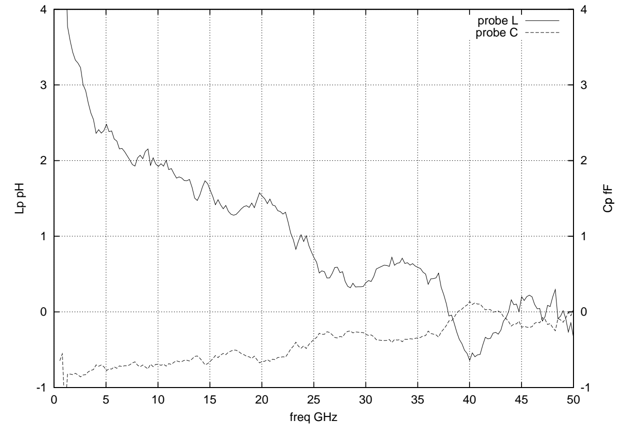

Figure 8: The extracted probe L and C, averaged over error box a and b, for the LRM/TLR trans-calibration error boxes. The probe tip LRM and TLR were performed on the same alumina calibration substrate. Remaining parasitics result from the approximate probe tip LRM and measurement error.

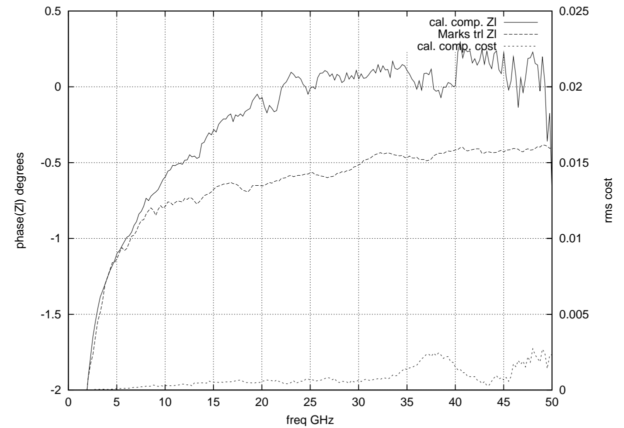

Figure 9: A comparison of the phase of the extracted line impedance using the new technique and the propagation constant method. The rms S-parameter difference between model and measurement is also shown. The TLR standards consist of 6 cpw lines, 50/25/200 μm strip/slot/ground plane wide and 197.4, 432.9, 870.9, 1736.8, 3383.1, 5080 μm long, fabricated on an alumina substrate. An initial probe tip LRM calibration was used as reference.

results from the new and the TLR/match method supports the made assumptions. Also, the low probe parasitics present in the LRM/TLR trans-calibration error boxes show that probe tip LRM, although approximative, is quite accurate, see fig. 8.

A comparison of the line impedance phase, estimated from the new technique and the propagation constant method of [2], see fig. 9, validates the new approach for low loss substrates.

The remaining difference may result from an inadequate error box model, here probably above 35 GHz, an increase in dielectric loss, assumed zero in [2], or non TE- or TM-

behaviour, which invalidates (1).

The on-wafer calibration structures consist of 0.5 μm thick Al 15/11/183 μm, strip/slot/ground plane, coplanar lines of 100, 340, 1300 and 6300 μm long, separated by a 1 μm thick dielectricum from a 5 S/m Si lossy substrate. Multi-line TLR was performed to obtain the error box data. Figure 10 summarizes the results, which are consistent with [10]. Especially the low frequency RC behaviour, up to 1 GHz, and the high loss transition between the slow-wave and the dielectric quasi-TEM mode, at 3 GHz, is clearly visible.

The series and parallel loss was calculated from

$$\gamma = \sqrt{(R+j\omega L)(G+j\omega C)} \tag{29}$$

$$\approx \frac{R}{2\Re(Z_l)} + \frac{G\Re(Z_l)}{2} + j\omega\sqrt{LC} \tag{30}$$

which holds if $\omega L \gg R$ and $\omega C \gg G$, since

$$Z_l = \sqrt{\frac{R+j\omega L}{G+j\omega C}} \tag{31}$$

$$\approx \sqrt{\frac{L}{C}}\left[1 + j\left(\frac{G}{2\omega C} - \frac{R}{2\omega L}\right)\right] \tag{32}$$

is then valid. The error in (30), for the here presented data, is below 1.5% above 1 GHz.

8 Conclusion

A robust line impedance identification method was presented. The method compares two calibrations and assumes that the difference is a symmetric error. Any nonsymmetry is thus attributed to a reference impedance change. The method is reflection parameter based and avoids any transformation into chain or transmission parameters.

Acknowledgment

The author is supported by the Institute for the Promotion of Innovation by Science and Technology in Flanders (IWT). D. Schreurs is supported by the Fund for Scientific Research (FWO). D. Vanhoenacker, Université Catholique de Louvain, is acknowledged for making available the measurements used to develop the presented technique. The reported data is from a silicon wafer designed and processed by IMEC.

References

[1] M.B. Marks, "A Multiline Method of Network Analyzer Calibration," *IEEE Transactions on Microwave Theory and Techniques,* Vol. 39, No. 7, July 1991, pp. 1205–1215.

[2] R. Marks, D. Williams, "Characteristic Impedance Determination Using Propagation Constant Measurement," *IEEE Microwave and Guided Wave Letters,* Vol. 1, No. 6, June 1991, pp. 141–143.

[3] G. Carchon, D. Schreurs, S. Vandenberghe, B. Nauwelaers, W. De Raedt, "Compensating differences between measurement and calibration wafer in probe tip calibrations - deembedding of line parameters," *1998 European Microwave Conference,* Amsterdam, October 1998, pp. 259–264.

[4] D. Williams, U. Arz, H. Grabinski, "Accurate Characteristic Impedance Measurement on Silicon," *IEEE MTT-S Digest,* 1998, pp. 1917–1920.

[5] R. Collin, "Foundations for Microwave Engineering," McGraw-Hill, New York, 1966.

[6] D. Williams, R. Marks, "Reciprocity Relations in Waveguide Junctions," *IEEE Transactions on Microwave Theory and Techniques,* Vol. 41, No. 6/7, June/July 1993, pp. 1105–1110.

[7] J. Brews, "Characteristic impedance of microstrip lines," *IEEE Transactions on Microwave Theory and Techniques,* Vol. 35, No. 1, Januari 1987, pp. 30–34.

[8] R. Pantoja, M. Howes, J. Richardson, R. Pollard, "Improved Calibration and Measurement of the Scattering Parameters of Microwave Integrated Circuits," *IEEE Transactions on Microwave Theory and Techniques,* Vol. 37, No. 11, November 1989, pp. 1675–1680.

[9] F. Lin, G. Kompa, "FET Model Parameter Extraction Based on Optimization With Multiplane Data-Fitting and Bidirectional Search–A New Concept," *IEEE Transactions on Microwave Theory and Techniques,* Vol. 42, No. 7, July 1994, pp. 1114–1121.

[10] E. Grotelüschen, L.S. Dutta, S. Zaage, "Quasi-analytical Analysis of the Broadband Properties of Multiconductor Transmission Lines on Semiconducting Substrates," *IEEE Transactions on Components, Packaging and Manufacturing Technology–Part B,* Vol. 17, No. 3, August 1994, pp. 376–382.

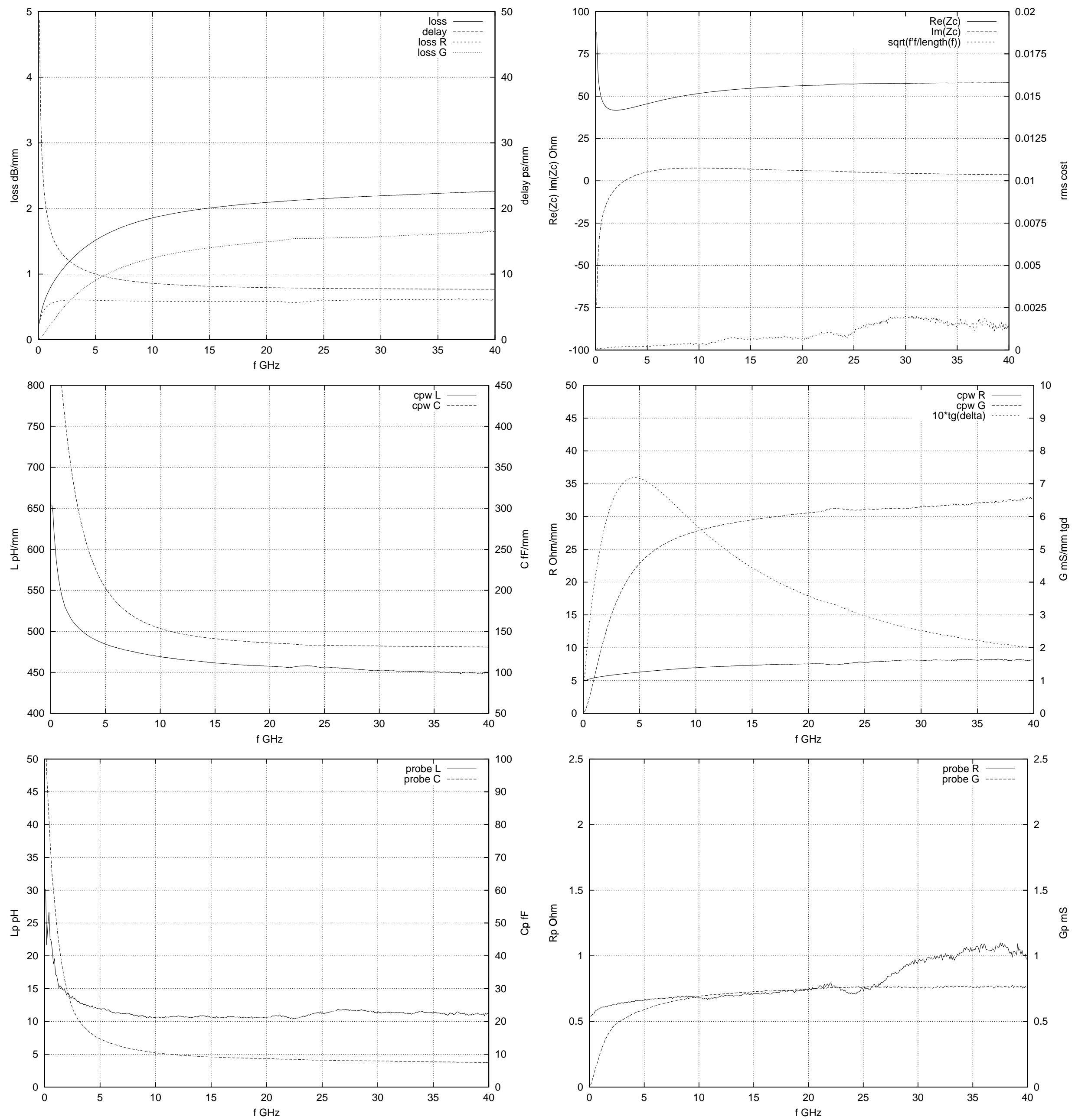

Figure 10: Top left: the line loss, delay, and the series and parallel loss calculated from the telegrapher's equation. Top right: the estimated line impedance and the error box fit cost. Center: the extracted line L, C and R, G,tgδ. Bottom: the total extracted probe L, C and R, G, averaged over error box a and b. All plots are for 0.5 μm thick Al 15/11/183 μm coplanar lines separated from a 5 S/m Si substrate by a 1 μm thick dielectricum. The lines were 100, 340, 1300 and 6300 μm long.